Supporting Information for: Particle Interactions in Liquid Magnetic Colloids by Zero Field Cooled Measurements: Effects on Heating Efficiency

P de la Presa[a,b], Y Luengo[c], V Velasco[a], MP Morales[c], M Iglesias[a], S Veintemillas-Verdaguer[c], P Crespo[a,b], A Hernando[a,b]

[(a)] Instituto de Magnetismo Aplicado (UCM-ADIF-CSIC), P.O. Box 155, Las Rozas, Madrid 28230, Spain

[(b)] Departamento de Física de Materiales, Univ. Complutense de Madrid, Plaza Ciencias 1, Madrid 28040, Spain

[(c)] Departamento de Biomateriales y Materiales Bioinspirados, Instituto de Ciencia de Materiales de Madrid/CSIC, Sor Juana Inés de la Cruz 3, Cantoblanco, Madrid 28049, Spain

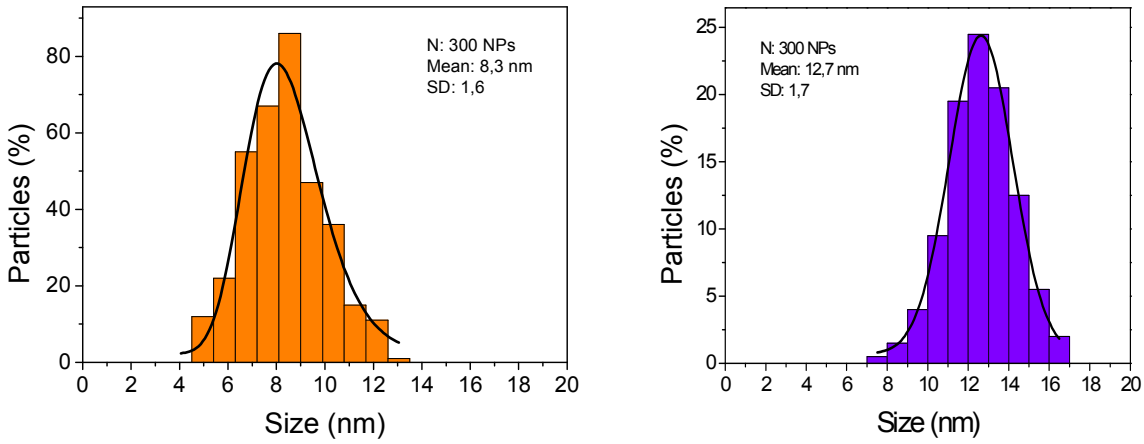

Figure S1. Size distribution of uncoated 8 nm (left) and 13 nm (right) MNPs (Reprinted adapted with permission from de la Presa et al., J. Phys Chem 116 (48), pp 25602–25610 (2012). Copyright (2012) American Chemical Society.)

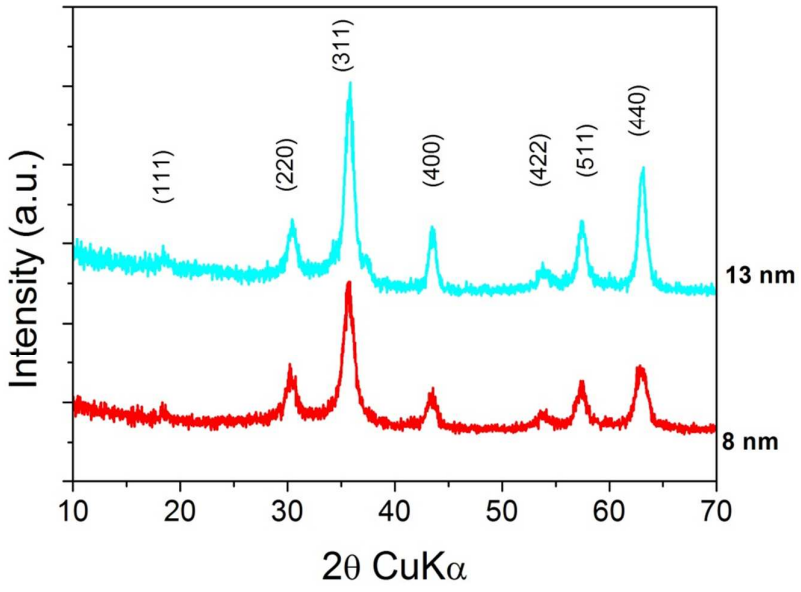

Figure S2. XRD pattern for the uncoated 8 and 13 nm NPs All diffraction peaks correspond to magnetite spinel crystalline phase (#PDF00-039-1346). (Reprinted adapted with permission from de la Presa et al., J. Phys Chem 116 (48), pp 25602–25610 (2012). Copyright (2012) American Chemical Society.)

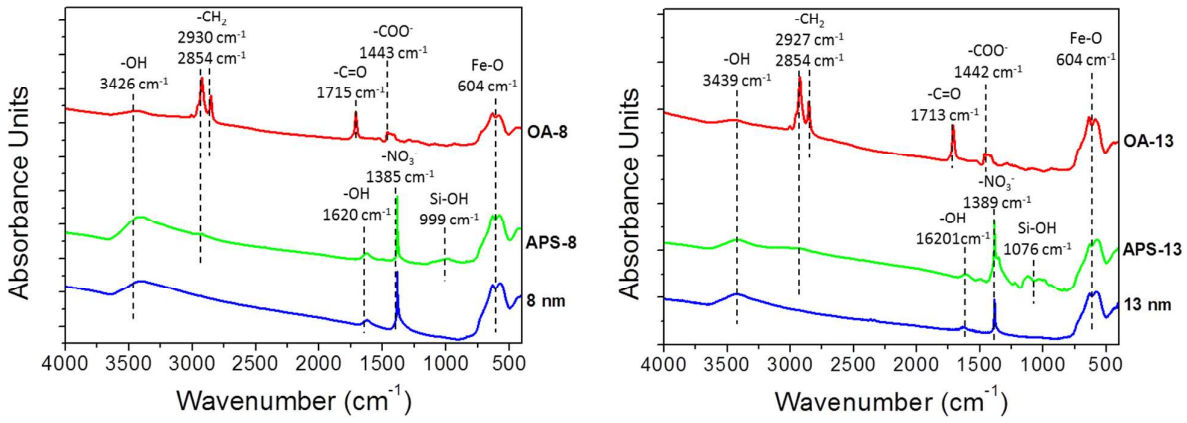

Figure S3. FTIR spectra of 8 and 13 nm NPs.

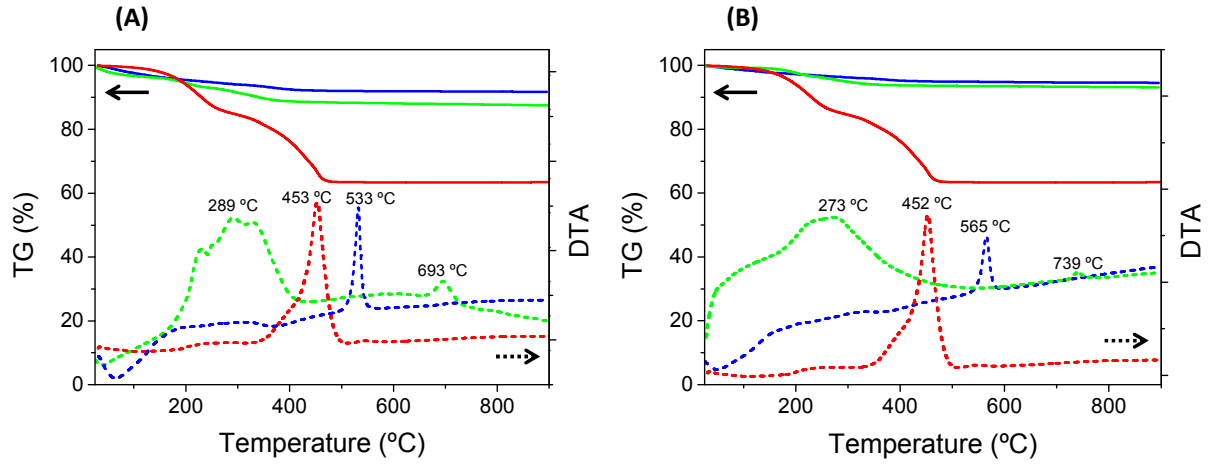

Figure S4. Results of DTA-TG analysis of: A) 8 nm (blue), APS-8 (green) and OA (red) and B) 13 nm (blue), APS-13 (green) and OA-13 (red).

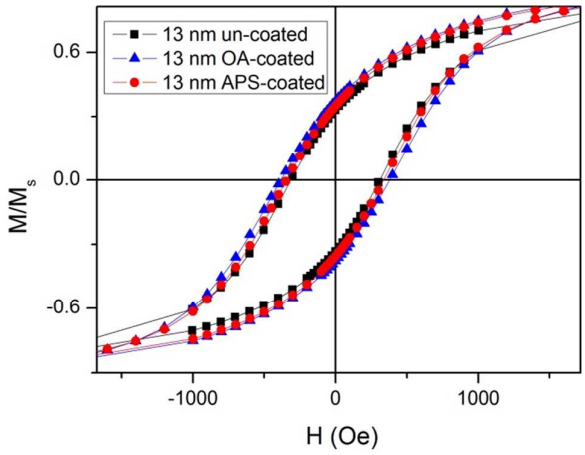

Figure S5: Magnetization curves at 5 K for OA-13 and APS-13 nm with concentrations 80 and 20 mg/ml, respectively, and uncoated-13 nm measured at 10 K with 50 mg/ml concentration (this last one is a reprint adapted with permission from de la Presa et al., J. Phys Chem 116 (48), pp 25602–25610 (2012). Copyright (2012) American Chemical Society).

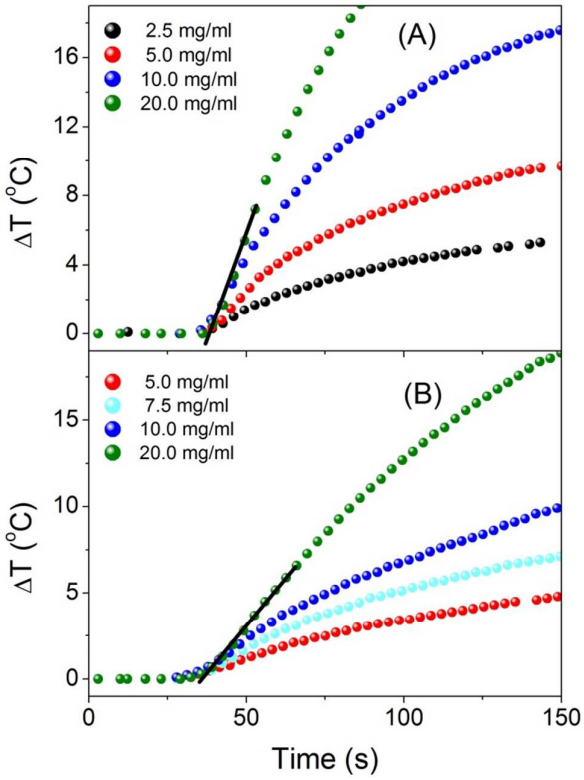

Figure S6: Heating curves for (A) OA-13 nanoparticles dispersed in hexane and (B) APS-13 nanoparticles in aqueous colloid under a magnetic field of 200 Oe and 110 kHz. The black straight lines represent the fits of the first seconds (~30 s) after turning the magnetic field on. For the sake of clarity, the rest of lines are not shown in the figure.

THE JOURNAL OF PHYSICAL CHEMISTRY C

Article

pubs.acs.org/JPCC

Particle Interactions in Liquid Magnetic Colloids by Zero Field Cooled Measurements: Effects on Heating Efficiency

P. de la Presa,*[,†,‡] Y. Luengo,[§] V. Velasco,[†] M. P. Morales,[§] M. Iglesias,[†] S. Veintemillas-Verdaguer,[§] P. Crespo,[†,‡] and A. Hernando[†,‡]

[†]Instituto de Magnetismo Aplicado (UCM-ADIF-CSIC), P.O. Box 155, Las Rozas, Madrid 28230, Spain

[‡]Departamento de Física de Materiales, Univ. Complutense de Madrid, Plaza Ciencias 1, Madrid 28040, Spain

[§]Departamento de Biomateriales y Materiales Bioinspirados, Instituto de Ciencia de Materiales de Madrid/CSIC, Sor Juana Inés de la Cruz 3, Cantoblanco, Madrid 28049, Spain

Supporting Information

ABSTRACT: The influence of magnetic interactions in assemblies formed by either aggregated or disaggregated uniform γ-Fe_2O_3 particles are investigated as a function of particle size, concentration, and applied field. Hyperthermia and magnetization measurements are performed in the liquid phase of colloids consisting of 8 and 13 nm uniform γ-Fe_2O_3 particles dispersed in water and hexane. Although hexane allows obtaining the disagglomerated particle system, aggregation is observed in the case of water colloids. The zero field cooled (ZFC) curves show a discontinuity in the magnetization values associated with the melting points of water and hexane. Additionally, for 13 nm γ-Fe_2O_3 dispersed in hexane, a second magnetization jump is observed that depends on particle concentration and shifts toward lower temperature by increasing applied field. This second jump is related to the strength of the magnetic interactions as it is only present in disagglomerated particle systems with the largest size, i.e., is not observed for 8 nm superparamagnetic particles, and surface effects can be discarded. The specific absorption rate (SAR) decreases with increasing concentration only for the hexane colloid, whereas for aqueous colloids, the SAR is almost independent of particle concentration. Our results suggest that, as a consequence of the magnetic interactions, the dipolar field acting on large particles increases with concentration, leading to a decrease of the SAR.

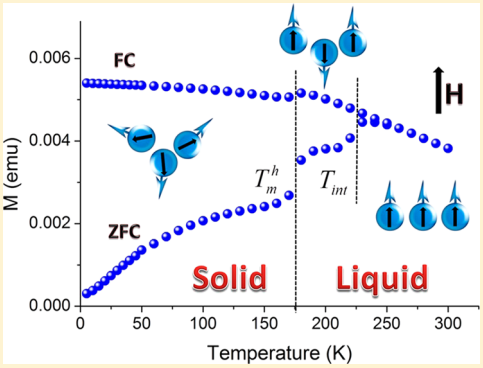

INTRODUCTION

The heating efficiency of magnetic nanoparticles under an alternating magnetic field wakes up the interest of the scientific community due to their applications in cancer treatments.[1−7] The aim of most research is to find biocompatible magnetic nanoparticles with high specific absorption rate (SAR) values that can be synthesized in large quantities in an easy, cheap, and reproducible way.[8] However, maximizing the SAR values and interpreting experimental results is a complex task as the SAR of magnetic nanoparticles assemblies depends on (i) magnetic particle properties (size, composition, anisotropy, surface, etc.), (ii) dispersion media properties (dielectric constant, hydrophobicity, and viscosity), and (iii) the combination of both that determines finally the interactions between particles. Among the large number of possible parameter variations, most investigations are devoted on modification of particle concentration as an attempt for understanding how the magnetic interactions could affect particle heating efficiency. Nevertheless, controversial behaviors are found in the literature.[8−13]

For an assembly of single domain noninteracting particles, the heating mechanism is now well understood.[14,15] However, for an assembly of interacting particles, the role of dipolar interactions on the heating efficiency is still under investigation.[9,10,16−19] Recently, the role of the dipolar interaction in the SARs has been analyzed by means of the mean-field model.[19] The results point out that the strong influence of the dipolar interactions has an unpredictable effect; i.e., depending on system parameters like magnetic anisotropy or applied field, the SAR could increase as well as decrease. In particular, when nanoparticles are small enough to clearly have superparamagnetic behavior, the influence of magnetic interactions is to increase the effective anisotropy.[20] However, when the magnetic behavior is at the limit of the superparamagnetic to ferromagnetic regimen, the influence of the interactions is not so clear and apparently contradictory results are found.[8−12]

In this work, we discuss the effects of dipolar interactions, observed through magnetic measurements, on the heating

Special Issue: Current Trends in Clusters and Nanoparticles Conference

Received: November 18, 2014
Revised: February 24, 2015
Published: February 25, 2015

DOI: 10.1021/jp5115515
J. Phys. Chem. C 2015, 119, 11022−11030

efficiency of 8 and 13 nm γ-Fe_2O_3 particles dispersed in hexane or water. Particle sizes below and above 10 nm allow the study of two different magnetic regimes: in the pure superparamagnetic regime and in the limit of superparamagnetic-ferromagnetic behavior. Furthermore, all the particles are synthesized by the coprecipitation method,[8,21] transformed to maghemite, and subsequently coated to obtain colloidal suspensions in water (aminopropylsilane coating) and in hexane (oleic acid coating). In this way, it is ensured that all the particles produced in a batch have the same structural and magnetic properties, independently of the dispersion media. Thus, the differences observed in the magnetic behavior should arise from surface effects and/or magnetic interactions.

The strength of the interactions is modified by using two dispersion media as well as by changing the particle concentration in the colloids. Particles dispersed in hexane are disaggregated and interparticle distances can be modified by varying the concentration, and when the dispersion medium is water, the particles have a clear tendency to form compact aggregates with constant interparticle distances within the aggregates. As will be shown, such interactions have a strong influence on the heating capabilities of the different colloidal systems.

EXPERIMENTAL METHODS

1. Synthesis. Maghemite nanoparticles are obtained by following a modified Massart coprecipitation protocol[22] as reported in ref 8. Briefly, magnetite (Fe_3O_4) nanoparticles are synthesized by adding of 425 mL of an aqueous solution of $FeCl_3{\cdot}6H_2O$ (0.09 mol) and $FeCl_2{\cdot}4H_2O$ (0.054 mol) to 75 mL of alkaline medium. The particle size can be tuned by the nature of the alkaline medium, the addition rate, and the aging time.[23] Thus, fast addition rates (40 mL/s) and NH_4OH (25%) as alkaline solutions are used to produce the 8 nm particles. Slow addition rates (0.2 mL/s) over NH_4OH (25%) followed by a heating process at 90 °C for 3 h are used to synthesize 13 nm particles. After every synthesis the particles are washed three times with distilled water and collected with the help of a permanent magnet.

1.1. Acid Treatment. A standard protocol is used to oxidize magnetite to maghemite (γ-Fe_2O_3).[21,25] In addition, this treatment activates the particle surface for further coating with aminopropylsilane (APS) groups. Briefly, 300 mL of HNO_3 (2 M) is added to 500 mL of the dispersion produced previously, and the mixture is stirred for 15 min. Then, the supernatant is removed by magnetic decantation and 75 mL of $Fe(NO_3)_3$ (1 M) and 130 mL of water are added to the particles. The mixture is heated to boiling temperature and stirred for 30 min.[21,24] The particles are then cooled to room temperature and, by magnetic decantation, the supernatant is substituted by 300 mL of HNO_3 (2 M) and the solution stirred for 15 min. Finally the particles are washed three times with acetone and redispersed in water. A rotary evaporator is used to remove any acetone waste as well as for concentrating the sample.

1.2. Aminopropylsilane (APS) Coating. APS coating has been proposed as an excellent material to stabilize magnetic nanoparticles at pH 7 and to provide positively charged groups at the nanoparticle surface that can be used to attach other biomolecules.[25] Surface modification is performed by adding very slowly (10 μL/s) 1.22 mL (0.005 mol) of (3-aminopropyl)triethoxysilane (APS) to a mixture of 10 mL of particles (28 mg Fe_2O_3/mL) and 10 mL of methanol, keeping strong stirring for 12 h. After that, methanol is eliminated in the rotary evaporator, and the rest of the APS is eliminated by dialysis (samples APS-8 and APS-13).

1.3. Oleic Acid (OA) Coating. Oleic acid is expected to stabilize the particles in hydrophobic organic media leading to full particle disaggregation. Surface modification is carried out by adding 640 mg of oleic acid to a colloid that contains 160 mg of Fe in 32 mL of water, keeping ultrasonic agitation at 70−80 °C for 1 h. After that, the sample is washed first with H_2O and then with ethanol and finally dried and redispersed in hexane (samples OA-8 and OA-13).

2. Structural and Colloidal Characterization. The crystalline structure of the samples before coating is identified by X-ray powder diffraction (XRD) performed in a Bruker D8 Advance powder diffractometer using Cu Kα radiation. The patterns are collected between 10° and 70°. The XRD spectra are indexed to an inverse spinel structure. The average crystallite size is calculated from the full width at half-maximum of the (311) diffraction peak by means of the diffraction computer program (APD) utilities from Phillips. The error in the crystallite sizes obtained by use of the Scherrer's equation is ±0.1 nm, which is related to the instrumental line broadening ($\Delta 2\theta$ = 0.11°).

Particle size and shape are determined by transmission electron microscopy (TEM) and high resolution electron microscopy (HRTEM). The mean particle size and distribution are evaluated by measuring the largest internal dimension of at least 100 particles. Afterward, data are fitted to a log-normal or Gaussian distribution to obtain the mean size and standard deviation (σ), which is considered to be representative of the absolute error of the measurement.

Fourier transform infrared spectra (FTIR) are recorded between 4000 and 400 cm^{-1} in a Bruker IFS 66 V-S spectrometer. Samples are prepared by dilution of iron oxide powder (2 wt %) in KBr and compressing the mixture into a pellet. Simultaneous thermogravimetric (TG) analysis and differential thermal analysis (DTA) are performed on a Seiko TG/DTA 320U thermobalance. Samples are heated from room temperature to 900 °C at 10 °C/min under an air flow of 100 mL/min.

Colloidal properties of the samples are studied in a Zetasizer Nano S, from Malvern Instruments. The hydrodynamic size of the particles in suspension is measured by dynamic light scattering (DLS) in intensity (Z-average) and in number. Larger aggregates have a contribution to the hydrodynamic size obtained from intensity data larger than in the case of the hydrodynamic size calculated in number. Each hydrodynamic value is the result of three different measurements at different dilutions to avoid errors coming from backscattering and using the scattering index for the solvent where the particles are dispersed, water or hexane.

The Fe concentration is measured with an inductively coupled plasma optical emission spectrometer (ICP-OES) PerkinElmer Optima 2100 DV. For this purpose samples are digested with nitric acid to oxidize the organic coating and then with hydrochloric acid to dissolve the particles.

3. Magnetic Characterization. The magnetic characterization is performed in a SQUID magnetometer Quantum Design MPMS-5S. Samples consisted on 50 μL of iron oxide suspension at different concentrations (2.5, 5, 10, 20, 50, and 80 mg/mL), introduced in special closed sample holders. Magnetization curves with a maximum applied field of 50 kOe have been measured at 5 and 250 K. Thermal dependence of

DOI: 10.1021/jp5115515
J. Phys. Chem. C 2015, 119, 11022−11030

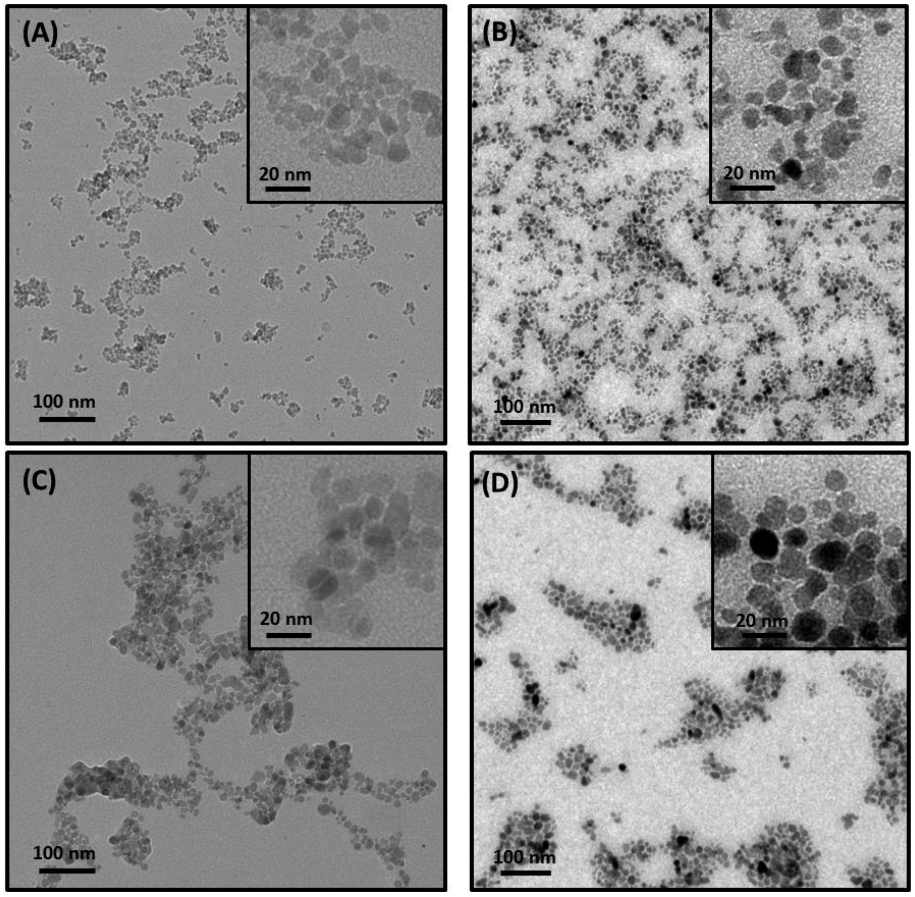

Figure 1. TEM micrographs of 8 nm γ-Fe_2O_3 coated with (A) APS and (B) OA and 13 nm γ-Fe_2O_3 coated with (C) APS and (D) OA.

Table 1. Experimental Results on Mean Particle Sizes Obtained by TEM and XRD and Hydrodynamic Size (D_h) and Mean Number at pH 7 before and after APS and OA Particle Coating As Characterized by DLS

			hydrodynamic size (nm)					
			uncoated (water)		APS-coated (water)		OA-coated (hexane)	
sample	TEM (nm)	XRD (nm)	Z-average[a]	mean number	Z-average	mean number	Z-average	mean number
8	8.3 (0.2)	7.9	47 (0.20)	33	54 (0.15)	37	14 (0.17)	9.5
13	12.7 (0.2)	12.3	60 (0.18)	34	76 (0.13)	40	22 (0.10)	15

[a]Polydispersity degree (standard deviation/mean size) is included in parentheses.

the magnetization under zero field cooled (ZFC) and field cooled (FC) conditions, from 5 to 300 K, has been measured by applying 50, 100, and 150 Oe magnetic fields. Diamagnetic contribution from water/hexane is subtracted from the experimental data.

4. Heating Efficiency. Heating capacities of nanoparticles are measured with the commercial system Magnetherm 1.5 (Nanotherics). The mean magnetic field inside the coil is measured with a two turns secondary coil with a cross-sectional value close to that of the sample holder (6.2 mm diameter). A half-length of the sample is made to coincide with the maximum value of the magnetic field. The volume sample is 1 mL. The temperatures of the coils are controlled through a closed circuit of water maintained at 16 °C with a cryostat bath.

The temperature of the colloids is measured with a fiberoptical thermometer and registered with a computer. Prior to turning the magnetic field on, the sample temperature is recorded for about 30 s to ensure thermal stability and to have a baseline for the calculation of the SAR. As the field is turned on, the temperature increase is measured either during 300 s or up to 80 °C for aqueous colloids and 40 °C for hexane colloids, well below the corresponding boiling temperatures 100 and 69 °C, respectively. By performing a linear fit of data (temperature versus time) in the initial time interval, we can obtain the slope $\Delta T/\Delta t$. As the measurements are performed in nonadiabatic conditions, the curve slopes $\Delta T/\Delta t$ are fitted only in the first few seconds after turning the magnetic field on. The time range is selected such as the slope is maximum, typically during the first 30 s.[26]

As the Fe concentrations are in the range 1−10 wt %, the SAR values can be calculated as SAR = $(C_{liq}/c_{Fe})(\Delta T/\Delta t)$, where C_{liq} is the specific heat capacity of water (4.185 J/(g K)) or hexane (2.28 J/(g K)) and c_{Fe} is the Fe weight concentration in the colloid.[27] Then, the SAR values are obtained by fitting the experimental heating curves and normalizing to the iron mass (W/g_{Fe}).

The SAR values of systems consisted of 8 and 13 nm particles coated with OA and APS are measured as a function of

DOI: 10.1021/jp5115515
J. Phys. Chem. C 2015, 119, 11022−11030

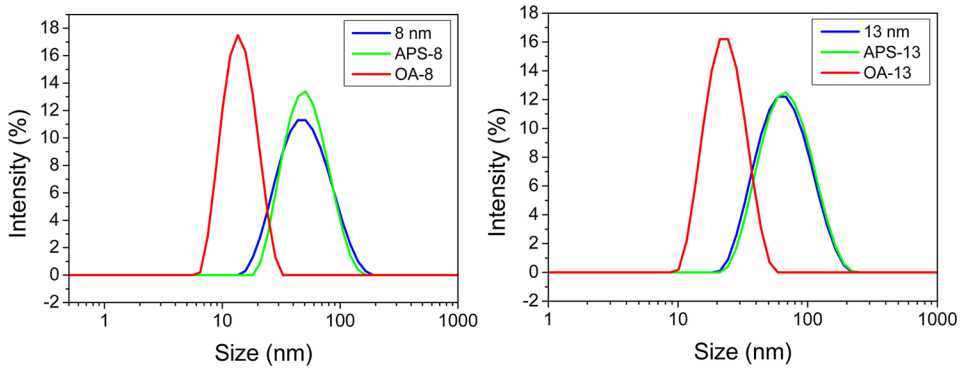

Figure 2. Hydrodynamic sizes of 8 and 13 nm uncoated (blue) and APS-coated (green) nanoparticles dispersed in water and of OA-coated (red) nanoparticles dispersed in hexane. Note the logarithmic scale.

iron concentration (c_{Fe}) at H = 200 Oe and f = 110 kHz. By starting with the highest concentrated sample, we performed subsequent measurements by diluting the samples in consecutive steps with milli-Q water for aqueous colloid and hexane for organic colloid and sonicating for several minutes.

The concentrations used for hyperthermia measurements are c_{Fe} = 20, 10, 7.5, 5, and 2.5 mg/mL. It should be mentioned that in the case of APS-coated nanoparticles, it has not been possible to obtain long time stable aqueous colloid for concentration larger than 20 mg/mL. For the maximum iron concentration, 20 mg/mL, the weight concentration is 2% wt; then, it is assumed that the heat capacity of the colloid is close to the heat capacity of the liquid carrier for all measurements.

RESULTS AND DISCUSSION

1. Structural and Colloidal Properties. Average particle size of uncoated nanoparticles are determined from TEM micrographs, as those shown in Figure 1, and the values are in agreement with those obtained from XRD diffractograms (see Table 1 and Figures S1 and S2 from the Supporting Information). All diffraction peaks correspond to maghemite spinel crystalline phase (#PDF00-039-1346). Diffraction peaks become broader as the nanoparticle size decreases from 13 to 8 nm, as expected.

For improving uniformity, crystallinity, and colloidal stability, the particles are subjected to an acid treatment. This allows a reduction of particle size distribution from 30% to 20% by dissolution of the smallest particles and by recrystallization of the largest ones, leading to highly crystalline particles with improved magnetic properties.[8,21] Hydrodynamic sizes of these uncoated particles at pH 7 are 47 and 60 nm for 8 and 13 nm particles, respectively.

The hydrodynamic size is only slightly altered by APS-coating (54 and 76 nm for 8 and 13 nm particles), whereas OA-coating is really effective in dispersing the particles reducing consequently the hydrodynamic sizes (14 and 22 nm for 8 and 13 nm) (Figure 2). It should be mentioned that hydrodynamic sizes in number for OA-coated samples (9.5 and 15 nm) fit to the TEM mean particle size plus the oleic acid chain length (1−2 nm) within the error. It can be concluded that although APS-coated particles form aggregates of different sizes stable in water, OA-coating disaggregates the nanoparticles leading to nearly individual particles stable in organic media (hexane). Table 1 summarizes the experimental results on particle sizes as well as the hydrodynamic sizes measured in water and hexane.

In the light of the FTIR and thermogravimetric results, APS and OA are strongly bonded to the particle surface (see Figures S3 and S4 in the Supporting Information). In addition to the bands between 700 and 400 cm^{-1}, which are attributable to maghemite, it is possible to observe a band for APS-coated particles at around 1000 cm^{-1} and a shoulder at 2930 cm^{-1}, which clearly correspond to the silanol groups at the particle surface of the APS-coated samples. OA-coated particles show characteristic IR bands that allow identification of the coating: 2928−2830 cm^{-1}, 1713 and 1457 cm^{-1}. Thermogravimetrical analysis also confirms the success of the coatings. A clear weight loss at 300−400 °C can be related to organic coating loss, being much more pronounced in the case of particles coated with OA (35%), due to its combustion, and the content of APS decreases only around 2−5% (see Figure S4A,B in the Supporting Information). These results support the idea that OA is able to coat individual particles, whereas APS coats particle clusters.

2. Magnetic Properties. *2.1. Magnetization Curves.* At low temperature, the hysteresis loops of the 8 and 13 nm OA- and APS-coated nanoparticles dispersed in hexane and water are close to that observed for uncoated nanoparticles (Figure S5, Supporting Information). Thus, it can be concluded that the coating processes do not affect the intrinsic magnetic properties of the particles.

Moreover, neither remanence (Mr/Ms ∼ 0.33) nor coercive field change with concentration (see Figure 3), contrary to that expected for an interacting particle system. To understand this apparent contradiction, we should look at the nanoparticle packing fraction, defined as the total volume occupied by the nanoparticles divided by the volume in which the nanoparticles

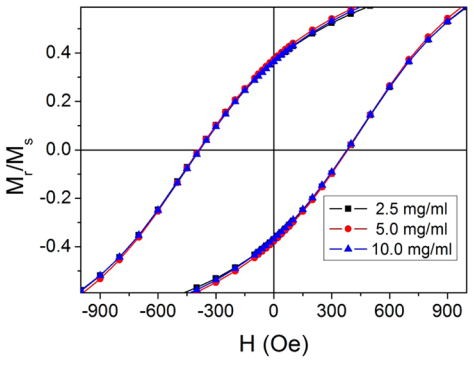

Figure 3. Hysteresis loops at 5 K of OA-13 dispersed in hexane at different concentrations. Diamagnetic contribution from hexane is extracted before normalization.

DOI: 10.1021/jp5115515
J. Phys. Chem. C 2015, 119, 11022−11030

are distributed. Then, the packing fraction runs from 0.10 to 0.30% when the particle concentration increases from 2.5 to 10 mg/mL. These values are indeed very small and it is known that, in the case of a system with large anisotropy values, remanence, coercive field, and blocking temperature are not significantly affected by dipolar interactions when packing fraction is below 1%.[28,29]

2.2. ZFC–FC in Aqueous Colloid. ZFC–FC curves of aqueous colloid measured up to 300 K show the effect of melting water (Figure 4). A jump in magnetization is observed as the temperature increases from 270 to 280 K that corresponds to the temperature transition between solid and liquid water.

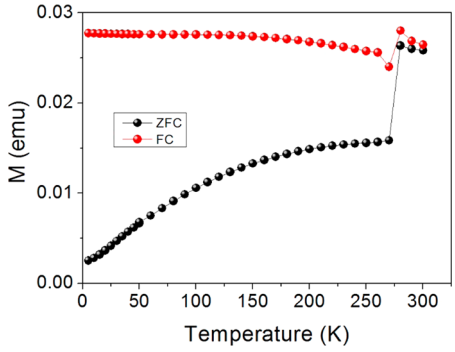

Figure 4. ZFC–FC curves of APS-13 aqueous colloid at c_{Fe} = 20 mg/mL. The sudden increase in magnetization occurs between 270 and 280 K. The applied field is 100 Oe.

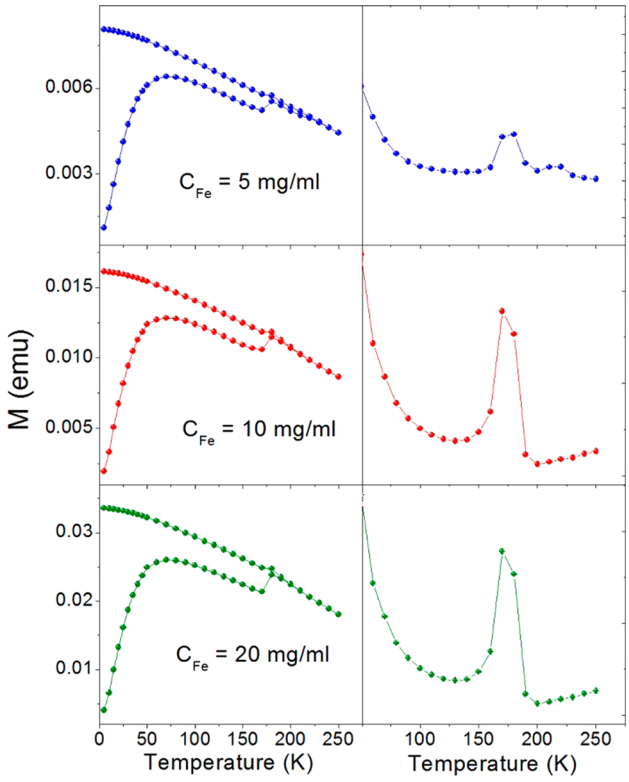

Figure 5. ZFC–FC measurements of OA-8 dispersed in hexane at 5 mg/mL (blue circles), 10 mg/mL (red circles), and 20 mg/mL (green circles) (left panel) and their corresponding derivatives (right panel).

As the ice melts (T_m^W = 273 K), the particles are free for rotating into the field direction, which gives rise to the observed magnetization jump. The observation of magnetization jump at melting temperature has been already reported for magnetic colloids in organic and aqueous media.[30,31]

2.3. ZFC–FC in Hexane Colloid. In the case of OA samples, a similar transition to that of the APS-13 aqueous colloid (in which the magnetization exhibits a discontinuous increase) is observed in ZFC curves at around T_m^H = 180 K, visible in both OA-13 and OA-8 nanoparticles. Additionally, 13 nm colloids exhibit a second transition temperature, T_{int}, above 200 K (Figures 5 and 6).

The first transition takes place at around the hexane melting point, T_m^H = 178 K; therefore, it can be associated with the liquid–solid phase transition of hexane, which allows the rotation of the particles into the field direction similar to that observed in aqueous colloids. For OA-8 nanoparticles having a blocking temperature around T_B = 70 K as a maximum observed in the ZFC curve, i.e., well below the melting temperature, the jump is due to the existence of a small fraction of particles that are still blocked inside the solid matrix. As the hexane melts, these particles are free to align with the field, which induces a sudden magnetization increase. It is worth noting that the magnetization increase at T_m^H is smaller for the OA-8 particles than for the OA-13 nanoparticles, supporting the statement that this increase is due to the physical rotation of nanoparticles as the hexane melts.

From Figures 5–7, it can be seen that, for concentrations smaller than 20 mg/mL, the melting temperature does not depend on the particle size, concentration, or applied field. At a very high particle concentration, the sample viscosity increases and the T_m^H jump is not observed, as the colloid has become bitumen with different properties from those of a colloid.[31]

The second transition temperature (T_{int}) observed in the ZFC–FC curves takes place at around 230 K for sample OA-13, and it is missed for OA-8. This magnetization jump depends on nanoparticle concentration as well as on applied field (see Figures 6 and 7):

i. NPs Concentration. There is no evidence of a second jump at low concentration, c_{Fe} = 2.5 mg/mL, and the jump shifts to higher temperatures (220–240 K) and becomes sharper with increasing concentration (c_{Fe} = 5–80 mg/mL).

ii. Applied Field. At 10 mg/mL, T_{int} gets smoother and shifts to lower temperatures with increasing magnetic field from 50 to 150 Oe, as can be seen from the derivative (Figure 7). For larger concentrations 80 mg/mL, T_{int} does not depend on the applied field.

Given that the T_{int} transition is not observed for the smallest nanoparticles, the surface effects, such as surfactant bonds, C–H dissociation of solvent molecules, viscosity inhomogeneity, or any other cause related to solvent or surfactant, can be discarded as causing the transition. It seems reasonable to think that such a transition should be more evident in the small particles due to their larger specific surface; this is not the case. Moreover, the fact that the transition temperature is affected by the applied field as well as by concentration and that this is only observed in a disaggregated particle system suggests that the dipolar interactions are in the origin of such effect.

The hydrodynamic sizes of OA-13 and OA-8 nanoparticles reflect the presence of individually-coated nanoparticles, i.e., the particles are disaggregated, and dilution increases the distance between particles. Therefore, the magnetic interactions vary with concentration and impact the magnetic properties. As can

DOI: 10.1021/jp5115515
J. Phys. Chem. C 2015, 119, 11022–11030

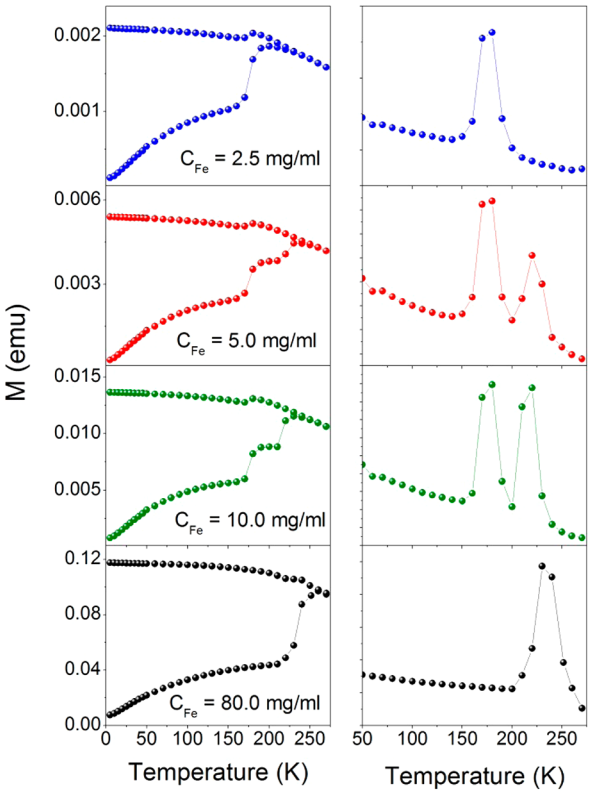

Figure 6. ZFC−FC curves at c_{Fe} = 2.5 mg/mL (blue circles), 5 mg/mL (red circles), 10 mg/mL (green circles), and 80 mg/mL (black circles) of OA-13 dispersed in hexane (left panel) and the corresponding ZFC curves derivatives (right panel). The ZFC−FC curves are measured at 100 Oe.

be seen from Figure 6, the transition is absent for very low concentrations, c_{Fe} = 2.5 mg/mL, whereas the magnetization jump increases with increasing concentration, i.e., decreasing particle distances, which confirms that this transition is mainly originated by the magnetic interactions.

Once the melting point of hexane is reached, the particles, which were embedded in a solid matrix with their easy axis pointing randomly, become unfrozen and are able to rotate into the field direction. However, when the applied magnetic field is smaller than the dipolar magnetic field acting on the particles, the minimization of the dipolar energy promotes the alignment parallel and antiparallel to the field direction. In the liquid phase, at temperatures between T_m^H and T_{int}, particles are free to rotate and align parallel and antiparallel to the field due to the dipolar interactions; above T_{int}, the energy barrier of the interactions is overcome by the thermal energy and all particle moments align with the applied field (see Figure 8). This is in agreement with the formation of nanoparticle chains or columns under application of ac magnetic field, which has been observed for other ferrofluids.[17,32−37]

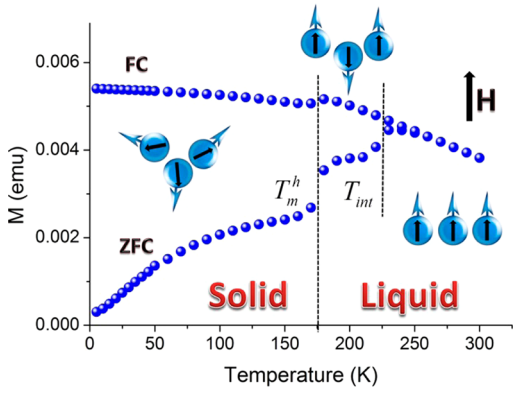

Figure 8. Scheme of magnetic moment orientation in ZFC curve for the OA-13 nanoparticles dispersed in hexane. (i) For $T < T_m^H$, the moments are randomly oriented in a solid matrix. (ii) For $T_m^H < T < T_{int}$, the particles are free to rotate and align parallel and antiparallel to the magnetic field due to the interactions. (iii) For $T > T_{int}$, the energy barrier is overcome by the thermal energy and all particle moments align toward the applied field.

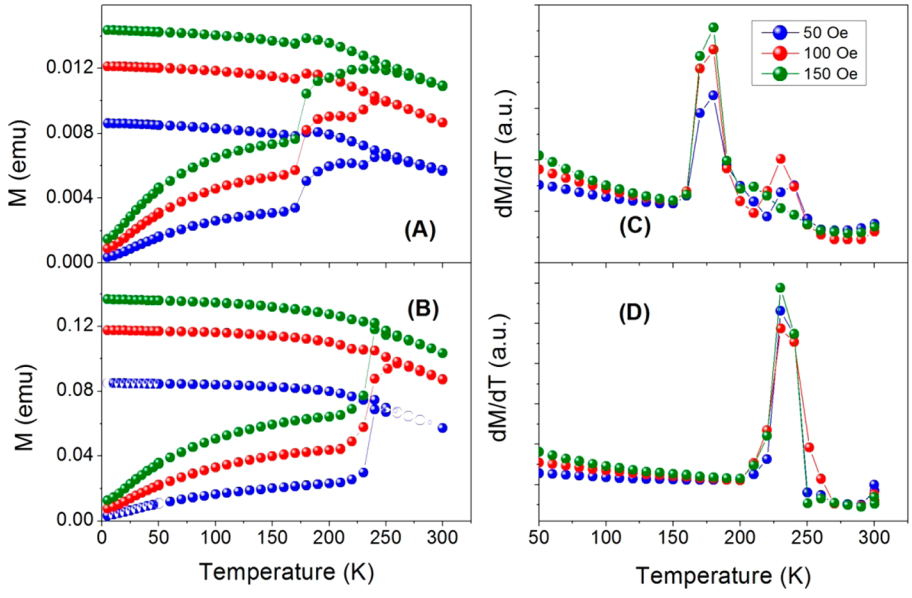

Figure 7. ZFC−FC curves at H = 50 (blue circles), 100 (red circles), and 150 Oe (green circles) of OA-13 dispersed in hexane at 10 mg/mL (A) and 80 mg/mL (B) and the corresponding ZFC curve derivatives (C,D).

DOI: 10.1021/jp5115515
J. Phys. Chem. C 2015, 119, 11022−11030

By calculating the thermal energy of the reversal process at $T_{int} \sim 230$ K, $E_{int} = k_B T \approx 3.2 \times 10^{-14}$ erg, and comparing it with a rough estimation of the energy of a magnetic nanoparticle with a mean size $d = 12.6$ nm placed in an external magnetic field $H_a = 150$ Oe, $M_s V H_a \approx 1.3 \times 10^{-14}$ erg, we observed that both energies are comparable. Thus, the energy needed to overcome the interparticle interactions is given either by the temperature (~230 K) or by the applied field ($H_a > 150$ Oe). According to these results, the dipolar field is around 150 Oe for $c_{Fe} = 10$ mg/mL and increases with concentration.

At this point a question arises: If the origin of such an effect is the dipolar interaction, why is it not observed in the OA-8 particles? The OA-8 particles exhibit a blocking temperature of around 70 K; thus, at temperatures above the hexane melting point, the thermal fluctuations are able to overcome the anisotropy barrier. In consequence, the magnetization of the particles is fluctuating and the dipolar field created by them also fluctuates, averaging to zero.

3. Heating Efficiency. One important issue limiting the application of the magnetic hyperthermia is the characteristics of the magnetic field required to produce the heating, which should be within the range approved for human use to avoid exceeding the discomfort factor limit $H_0 f < 5 \times 10^9$ A·m^{-1}·s^{-1}.[2,38,39] In this work, the product of applied field frequency and amplitude satisfies this condition.

Table 2 shows the results of fitting the heating curves shown in Figure 9, i.e., the slope $\Delta T/\Delta t$ and the calculated SAR values

Table 2. Results of the Fits of the Heating Curves: Particles, Liquid Heating Capacity (C_{liq}), Iron Concentration, Average Slope Values $\Delta T/\Delta t$, and Calculated SAR Values

particles	C_{liq} [(J/(g K)]	concentration (g Fe/mL)	$\Delta T/\Delta t$ (K/s)	SAR (W/g)
13 nm OA (in hexane)	2.28	0.020	0.53(3)[a]	61(3)
		0.010	0.34(3)	78(3)
		0.005	0.21(1)	95(5)
		0.0025	0.10(1)	96(7)
13 nm APS (in water)	4.18	0.020	0.25(2)	51(3)
		0.010	0.13(1)	54(3)
		0.0075	0.10(1)	56(4)
		0.005	0.07(1)	58(5)

[a]Average error is included in parentheses.

for each sample at a given concentration; Figure S6 in the Supporting Information shows an example of the time range used for the linear fit. As can be seen from Figure 9, ΔT increases with increasing iron concentration (Figure 9A,B) and, additionally, for the same iron concentration, ΔT increases faster for hexane colloids than for aqueous colloids due to the smaller heat capacity of hexane ($C_{hex} = 2.28$ J/(g K), $C_{water} = 4.18$ J/(g K)) (compare panels A and B of Figure 9). Given that the SAR is normalized to the different media heat capacities, it should be independent of the colloid media. However, the SAR in aqueous colloids is almost concentration independent whereas the SAR in hexane decreases noticeably as concentration increases; at 5 mg/mL the SAR in hexane is 95 W/g, 71% higher than the SAR in an aqueous colloid (56 W/g), and both values tend to approach each other with increasing concentration (see Table 2 and Figure 10).

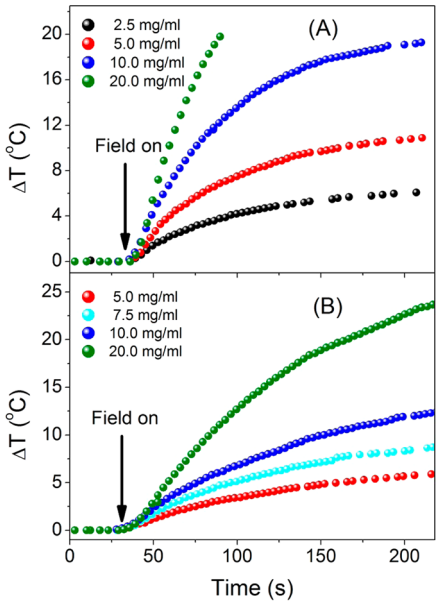

Figure 9. Temperature increases for 13 nm nanoparticles at different concentrations for (A) OA-coated dispersed in hexane and (B) APS-coated dispersed in water. The concentrations are 2.5 mg/mL (black circle), 5 mg/mL (red circles), 7.5 mg/mL (light blue circles), 10 mg/mL (blue circles), and 20 mg/mL (green circles). The applied field is $f = 110$ kHz and $H_0 = 200$ Oe. The arrows indicate the instant the magnetic field is turned on.

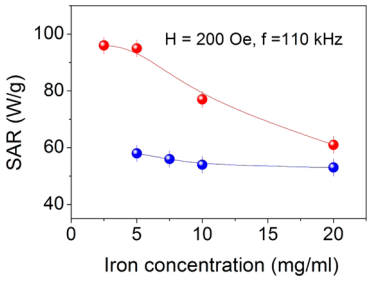

Figure 10. SAR dependence on iron concentration at $H_0 = 200$ Oe and $f = 110$ kHz for APS-13 (blue circles) and OA-13 (red circles) nanoparticles dispersed in water and hexane, respectively.

As the particles in hexane and water are produced in the same batch and the coating does not bear significantly on the magnetic properties, the interactions between particles seems to be responsible for the different heating efficiencies in OA- and APS-coated particles. In the case of APS-coated nanoparticles, the magnetic interactions between nanoparticles inside a cluster should not vary with particle concentration given that the SAR values are almost concentration independent (see Figure 10). In the case of OA-coated nanoparticles, the SAR decreases as the concentration rises. This result suggests that the interactions make the effective field acting on a particle drop off and go to a minimum at high concentrations, leading to similar low SAR values for all samples.

The aggregate state plays a fundamental role in the understanding of magnetic interactions taking place in a magnetic colloid. Thus, samples APS-8 and APS-13 are formed by the clusters composed of around 50−200 particles as indicated by the hydrodynamic radius values, whose aggregation state is determined by the synthesis. The subsequent dilution and sonication of the aqueous colloid cannot separate

DOI: 10.1021/jp5115515
J. Phys. Chem. C 2015, 119, 11022−11030

the particles inside the cluster but increase intercluster distances. Therefore, the magnetic interaction between nanoparticles inside the clusters should remain almost constant independent of particle concentration and, consequently, SAR values should not vary with concentration, as observed in Figure 10.

CONCLUSIONS

Hexane and water colloids of 8 and 13 nm maghemite nanoparticles have been obtained. Water colloids are formed by clusters of 50−200 nanoparticles whereas the use of hexane media leads to dispersed nanoparticles. Thermal dependence of the magnetization exhibits magnetization jumps that are related to the melting points of colloidal media as well as to the dipolar interactions among nanoparticles. The latter can be tuned by means of the colloidal media, particle size, and particle concentration in the colloid and the applied field. Hexane colloids formed by dispersed OA-13 nanoparticles exhibit a clear magnetization jump at temperatures above the melting point of hexane that is not observed for superparamagnetic OA-8 particles. This magnetization discontinuity appears for concentrations higher than 5 mg/mL and shifts toward lower temperatures with increasing applied field up to 150 Oe, indicating that dipolar interactions are on the origin of such behavior. The possible particle moment configuration is proposed as follows: (i) For $T < T_m$, the moments are randomly oriented in a solid matrix. (ii) For $T_m < T < T_{int}$, the particles are free to rotate in the liquid media. Not all particles rotate into the field direction due to the role played by the dipolar interaction. (iii) For $T > T_{int}$, the energy barrier due to the interactions is overcome by the thermal energy and all particle moments align toward the applied field. According to this, a maximum in the SAR would be expected at temperatures around T_{int}. For OA-8 particles, the dipolar field fluctuates and averages to 0; thus no transition associated with dipolar interaction is observed.

Additionally, it is observed that SAR values decrease when going from a noninteracting to an interacting system by increasing concentration. On the one hand, the increasing strength of the dipolar interaction promotes that the effective field acting on the particles decreases, thus being less effective for heating purposes. On the other hand, for the particles in an aqueous colloid the magnetic interactions are independent of the particle concentration; consequently, the SAR is constant with concentration.

ASSOCIATED CONTENT

Supporting Information

Additional figures from the TEM, XRD, SQUID, FTIR, heating curves, and DTA-TG experimental characterization of particles. This material is available free of charge via the Internet at http://pubs.acs.org.

AUTHOR INFORMATION

Corresponding Author

*P.d.l.P. E-mail: pmpresa@ucm.es.

Notes

The authors declare no competing financial interest.

ACKNOWLEDGMENTS

This work was supported by grants from the Spanish Ministry of Science and Innovation, MAT2012-37109-C02-01 and MAT2011-23641, Madrid Regional Government, S009/MAT-1726, and Fundación Mutua Madrileña (Spain).

DEDICATION

In memoriam Patricia Crespo.

REFERENCES

(1) Maier-Hauff, K.; Ulrich, F.; Nestler, D.; Niehoff, H.; Wust, P.; Thiesen, B.; Orawa, H.; Budach, V.; Jordan, A. Efficacy and Safety of Intratumoral Thermotherapy Using Magnetic Iron-Oxide Nanoparticles Combined with External Beam Radiotherapy on Patients with Recurrent Glioblastoma Multiforme. *J. Neuro-Oncol.* **2011**, *103*, 317−324.

(2) Johannsen, M.; Thiesen, B.; Wust, P.; Jordan, A. Magnetic Nanoparticle Hyperthermia for Prostate Cancer. *Int. J. Hyperthermia* **2010**, *26*, 790−795.

(3) Kolosnjaj-Tabi, J.; Di Corato, R.; Lartigue, L.; Marangon, I.; Guardia, P.; Silva, A. K. A.; Luciani, N.; Clement, O.; Flaud, P.; Singh, J. V.; et al. Heat-Generating Iron Oxide Nanocubes: Subtle "Destructurators" of the Tumoral Microenvironment. *ACS Nano* **2014**, *8*, 4268−4283.

(4) Sanchez, C.; Diab, D. E.; Connord, V.; Clerc, P.; Meunier, E.; Pipy, B.; Payre, B.; Tan, R. P.; Gougeon, M.; Carrey, J.; et al. Targeting a G-Protein-Coupled Receptor Overexpressed in Endocrine Tumors by Magnetic Nanoparticles to Induce Cell Death. *ACS Nano* **2014**, *8*, 1350−1363.

(5) Villanueva, A.; de la Presa, P.; Alonso, J. M.; Rueda, T.; Martinez, A.; Crespo, P.; Morales, M. P.; Gonzalez-Fernandez, M. A.; Valdes, J.; Rivero, G. Hyperthermia Hela Cell Treatment with Silica-Coated Manganese Oxide Nanoparticles. *J. Phys. Chem. C* **2010**, *114*, 1976−1981.

(6) Hervault, A.; Thanh, N. T. K. Magnetic Nanoparticle-Based Therapeutic Agents for Thermo-Chemotherapy Treatment of Cancer. *Nanoscale* **2014**, *6*, 11553−11573.

(7) Silvio, D.; Rudolf, H. Magnetic Particle Hyperthermia—a Promising Tumour Therapy? *Nanotechnology* **2014**, *25*, 452001.

(8) de la Presa, P.; Luengo, Y.; Multigner, M.; Costo, R.; Morales, M. P.; Rivero, G.; Hernando, A. Study of Heating Efficiency as a Function of Concentration, Size, and Applied Field in γ-Fe_2O_3 Nanoparticles. *J. Phys. Chem. C* **2012**, *116*, 25602−25610.

(9) Serantes, D.; Baldomir, D.; Martinez-Boubeta, C.; Simeonidis, K.; Angelakeris, M.; Natividad, E.; Castro, M.; Mediano, A.; Chen, D.-X.; Sanchez, A.; et al. Influence of Dipolar Interactions on Hyperthermia Properties of Ferromagnetic Particles. *J. Appl. Phys.* **2010**, *108*, 073918.

(10) Haase, C.; Nowak, U. Role of Dipole-Dipole Interactions for Hyperthermia Heating of Magnetic Nanoparticle Ensembles. *Phys. Rev. B: Solid State* **2012**, *85*, 045435.

(11) Piñeiro-Redondo, Y.; Bañobre-López, M.; Pardiñas-Blanco, I.; Goya, G.; López-Quintela, M.; Rivas, J. The Influence of Colloidal Parameters on the Specific Power Absorption of Paa-Coated Magnetite Nanoparticles. *Nanoscale Res. Lett.* **2011**, *6*, 1−7.

(12) Martinez-Boubeta, C.; Simeonidis, K.; Serantes, D.; Conde-Leborán, I.; Kazakis, I.; Stefanou, G.; Peña, L.; Galceran, R.; Balcells, L.; Monty, C.; et al. Adjustable Hyperthermia Response of Self-Assembled Ferromagnetic Fe-MgO Core−Shell Nanoparticles by Tuning Dipole−Dipole Interactions. *Adv. Funct. Mater.* **2012**, *22*, 3737−3744.

(13) Verges, M. A.; Costo, R.; Roca, A. G.; Marco, J. F.; Goya, G. F.; Serna, C. J.; Morales, M. P. Uniform and Water Stable Magnetite Nanoparticles with Diameters around the Monodomain-Multidomain Limit. *J. Phys. D: Appl. Phys.* **2008**, *41*, 134003.

(14) Carrey, J.; Mehdaoui, B.; Respaud, M. Simple Models for Dynamic Hysteresis Loop Calculations of Magnetic Single-Domain Nanoparticles: Application to Magnetic Hyperthermia Optimization. *J. Appl. Phys.* **2011**, *109*, 083921.

(15) Usov, N. A. Low Frequency Hysteresis Loops of Superparamagnetic Nanoparticles with Uniaxial Anisotropy. *J. Appl. Phys.* **2010**, *107*, 123909.

DOI: 10.1021/jp5115515
J. Phys. Chem. C 2015, 119, 11022−11030

(16) Mehdaoui, B.; Meffre, A.; Carrey, J.; Lachaize, S.; Lacroix, L. M.; Gougeon, M.; Chaudret, B.; Respaud, M. Optimal Size of Nanoparticles for Magnetic Hyperthermia: A Combined Theoretical and Experimental Study. *Adv. Funct. Mater.* **2011**, *21*, 4573−4581.
(17) Mehdaoui, B.; Tan, R. P.; Meffre, A.; Carrey, J.; Lachaize, S.; Chaudret, B.; Respaud, M. Increase of Magnetic Hyperthermia Efficiency Due to Dipolar Interactions in Low-Anisotropy Magnetic Nanoparticles: Theoretical and Experimental Results. *Phys. Rev. B: Solid State* **2013**, *87*, 174419.
(18) Garaio, E.; Sandre, O.; Collantes, J. M.; Garcia, J. A.; Mornet, S.; Plazaola, F. Specific Absorption Rate Dependence on Temperature in Magnetic Field Hyperthermia Measured by Dynamic Hysteresis Losses (AC Magnetometry). *Nanotechnology* **2015**, *26*, 015704.
(19) Landi, G. T. Role of Dipolar Interaction in Magnetic Hyperthermia. *Phys. Rev. B: Solid State* **2014**, *89*, 014403.
(20) Burrows, F.; Parker, C.; Evans, R. F. L.; Hancock, Y.; Hovorka, O.; Chantrell, R. W. Energy Losses in Interacting Fine-Particle Magnetic Composites. *J. Phys. D: Appl. Phys.* **2010**, *43*, 474010.
(21) Costo, R.; Bello, V.; Robic, C.; Port, M.; Marco, J. F.; Morales, M. P.; Veintemillas-Verdaguer, S. Ultrasmall Iron Oxide Nanoparticles for Biomedical Applications: Improving the Colloidal and Magnetic Properties. *Langmuir* **2012**, *28*, 178−185.
(22) Massart, R. Preparation of Aqueous Magnetic Liquids in Alkaline and Acidic Media. *IEEE Trans. Magn.* **1981**, *17*, 1247−1248.
(23) Morales, M. P.; Veintemillas-Verdaguer, S.; Montero, M. I.; Serna, C. J.; Roig, A.; Casas, L.; Martinez, B.; Sandiumenge, F. Surface and Internal Spin Canting in Gamma- Fe_2O_3 Nanoparticles. *Chem. Mater.* **1999**, *11*, 3058−3064.
(24) van Ewijk, G. A.; Vroege, G. J.; Philipse, A. P. Convenient Preparation Methods for Magnetic Colloids. *J. Magn. Magn. Mater.* **1999**, *201*, 31−33.
(25) Gazeau, F.; Levy, M.; Wilhelm, C. Optimizing Magnetic Nanoparticle Design for Nanothermotherapy. *Nanomedicine (London, U. K.)* **2008**, *3*, 831−844.
(26) Natividad, E.; Castro, M.; Mediano, A. Adiabatic vs. Non-Adiabatic Determination of Specific Absorption Rate of Ferrofluids. *J. Magn. Magn. Mater.* **2009**, *321*, 1497−1500.
(27) Gonzalez-Fernandez, M. A.; Torres, T. E.; Andres-Verges, M.; Costo, R.; de la Presa, P.; Serna, C. J.; Morales, M. R.; Marquina, C.; Ibarra, M. R.; Goya, G. F. Magnetic Nanoparticles for Power Absorption: Optimizing Size, Shape and Magnetic Properties. *J. Solid State Chem.* **2009**, *182*, 2779−2784.
(28) Dutz, S.; Hergt, R. The Role of Interactions in Systems of Single Domain Ferrimagnetic Iron Oxide Nanoparticles. *J. Nano—Electron. Phys.* **2012**, *4*, 02010.
(29) Abbasi, A. Z.; Gutierrez, L.; del Mercato, L. L.; Herranz, F.; Chubykalo-Fesenko, O.; Veintemillas-Verdaguer, S.; Parak, W. J.; Morales, M. P.; Gonzalez, J. M.; Hernando, A.; et al. Magnetic Capsules for NMR Imaging: Effect of Magnetic Nanoparticles Spatial Distribution and Aggregation. *J. Phys. Chem. C* **2011**, *115*, 6257−6264.
(30) Di Corato, R.; Espinosa, A.; Lartigue, L.; Tharaud, M.; Chat, S.; Pellegrino, T.; Menager, C.; Gazeau, F.; Wilhelm, C. Magnetic Hyperthermia Efficiency in the Cellular Environment for Different Nanoparticle Designs. *Biomaterials* **2014**, *35*, 6400−6411.
(31) Borin, D. Y.; Odenbach, S. Magnetic Measurements on Frozen Ferrofluids as a Method for Estimating the Magnetoviscous Effect. *J. Phys: Condens. Matter* **2009**, *21*, 246002.
(32) Saville, S. L.; Qi, B.; Baker, J.; Stone, R.; Camley, R. E.; Livesey, K. L.; Ye, L.; Crawford, T. M.; Thompson Mefford, O. The Formation of Linear Aggregates in Magnetic Hyperthermia: Implications on Specific Absorption Rate and Magnetic Anisotropy. *J. Colloid Interface Sci.* **2014**, *424*, 141−151.
(33) Klokkenburg, M.; Erné, B. H.; Meeldijk, J. D.; Wiedenmann, A.; Petukhov, A. V.; Dullens, R. P. A.; Philipse, A. P. In situ Imaging of Field-Induced Hexagonal Columns in Magnetite Ferrofluids. *Phys. Rev. Lett.* **2006**, *97*, 185702.
(34) Serantes, D.; Simeonidis, K.; Angelakeris, M.; Chubykalo-Fesenko, O.; Marciello, M.; Morales, M. d. P.; Baldomir, D.; Martinez-Boubeta, C. Multiplying Magnetic Hyperthermia Response by Nanoparticle Assembling. *J. Phys. Chem. C* **2014**, *118*, 5927−5934.
(35) Lacroix, L.-M.; Malaki, R. B.; Carrey, J.; Lachaize, S.; Respaud, M.; Goya, G. F.; Chaudret, B. Magnetic Hyperthermia in Single-Domain Monodisperse Feco Nanoparticles: Evidences for Stoner−Wohlfarth Behavior and Large Losses. *J. Appl. Phys.* **2009**, *105*, 023911.
(36) Meffre, A.; Lachaize, S.; Gatel, C.; Respaud, M.; Chaudret, B. Use of Long Chain Amine as a Reducing Agent for the Synthesis of High Quality Monodisperse Iron(0) Nanoparticles. *J. Mater. Chem.* **2011**, *21*, 13464−13469.
(37) Meffre, A.; Mehdaoui, B.; Kelsen, V.; Fazzini, P. F.; Carrey, J.; Lachaize, S.; Respaud, M.; Chaudret, B. A Simple Chemical Route toward Monodisperse Iron Carbide Nanoparticles Displaying Tunable Magnetic and Unprecedented Hyperthermia Properties. *Nano Lett.* **2012**, *12*, 4722−4728.
(38) Wust, P.; Gneveckow, U.; Johannsen, M.; Bohmer, D.; Henkel, T.; Kahmann, F.; Sehouli, J.; Felix, R.; Ricke, J.; Jordan, A. Magnetic Nanoparticles for Interstitial Thermotherapy—Feasibility, Tolerance and Achieved Temperatures. *Int. J. Hyperthermia* **2006**, *22*, 673−685.
(39) Hergt, R.; Dutz, S. Magnetic Particle Hyperthermia—Biophysical Limitations of a Visionary Tumour Therapy. *J. Magn. Magn. Mater.* **2007**, *311*, 187−192.

DOI: 10.1021/jp5115515
J. Phys. Chem. C 2015, 119, 11022−11030